Crystalline TiO 2 : A Generic and Effective Electron Conducting Protection Layer for Photo-anodes and -Cathodes

ARTICLE *in* THE JOURNAL OF PHYSICAL CHEMISTRY C · JUNE 2015

Impact Factor: 4.77 · DOI: 10.1021/acs.jpcc.5b04407

8 AUTHORS, INCLUDING:

Bastian Mei
Technical University of Denmark

Thomas Pedersen
Technical University of Denmark

Dowon Bae
Technical University of Denmark

THE JOURNAL OF PHYSICAL CHEMISTRY C

Article

pubs.acs.org/JPCC

Crystalline TiO_2: A Generic and Effective Electron-Conducting Protection Layer for Photoanodes and -cathodes

Bastian Mei,[†] Thomas Pedersen,[‡] Paolo Malacrida,[†] Dowon Bae,[†] Rasmus Frydendal,[†] Ole Hansen,[‡] Peter C. K. Vesborg,[†] Brian Seger,[†] and Ib Chorkendorff*,[†]

[†]Department of Physics, CINF, and [‡]Department of Micro- and Nanotechnology, Technical University of Denmark, DK-2800 Kongens Lyngby, Denmark

Supporting Information

ABSTRACT: Stabilizing efficient photoabsorbers for solar water splitting has recently shown significant progress with the development of various protection layers. Suitable protection layers for tandem devices should be conductive, transparent, and stable in strongly acidic or alkaline solutions. This paper shows that under certain conditions n-type semiconductors, such as TiO_2, can be used as protection layers for Si-based photoanodes. It also provides evidence that even in a photoanode assembly TiO_2 is conducting only electrons (not holes as in p-type protection layers), and therefore TiO_2 can be described as a simple ohmic contact. This renders n-type semiconductors, such as TiO_2, to be versatile and simple protection layers, which can be used for photoanodes and as previously shown for photocathodes. The ohmic behavior of n-type TiO_2 in a Si/TiO_2–photoanode assembly is demonstrated under dark and illuminated conditions by performing the oxygen evolution reaction (OER) and using the Fe(II)/Fe(III) redox couple. These measurements reveal that the performance of the Si/TiO_2–photoanode assembly is strongly dependent on the TiO_2/electrolyte interaction. Finally, the conditions and requirements that make TiO_2 generally applicable for photoanode assemblies, and thus for protecting tandem devices, are outlined and quantitatively shown by band diagram calculations. The results presented here provide the understanding required for the design of highly efficient and stable photoelectrochemical water splitting devices.

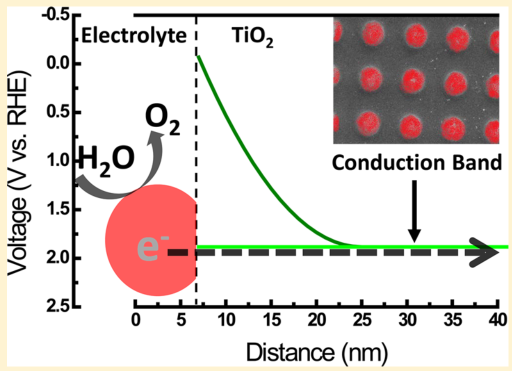

■ INTRODUCTION

Implementing clean processes for power generation is immensely important to secure future energy supply and to ensure sustainable economic growth.[1−3] Fortunately, the sun's energy supply (3×10^{24} joules per year) exceeds mankind's annual energy consumption by about 5000 times.[1,4] Utilizing sunlight to convert energy-poor to energy-rich molecules is a promising technology,[2−5] and rapid progress has been made in the field of photoelectrochemical splitting of water.[6−10] However, for tandem photoelectrochemical cells consisting of two matching photon absorbers, that is, large and small band gap materials,[11,12] a current bottleneck is the identification of optimal photon absorbers with suitable band gaps, favorable absorption properties, and feasible charge carrier motilities. Generally, these efficient photon absorbers are unstable in oxidizing environments, and establishing a successful strategy for the protection of efficient photon absorbers, such as Si[12] or III−V compounds,[7] against corrosion is therefore one of the key challenges for the production of solar fuels in a highly efficient tandem device where the efficiency is sought to be 10%.[6,8−10,13−15]

Titanium dioxide was already shown to be suitable to protect photocathodes due to its intrinsic n-type semiconducting behavior,[14] the suitable alignment of the conduction band edge with the hydrogen redox potential, and good optical properties.[14,16−18] Considering similar requirements for an anode protection layer, the number of available p-type (hole conducting) semiconductors is limited.[14,19] Instead, very thin films of various metals and metal oxide layers with reasonable transparency have been investigated as anodic protection layers.[6,10,15,20] Interestingly, Hu et al.[8] recently reported that a Ni-influenced transparent, thick amorphous TiO_2 protection layer is applicable for the protection of photoanodes. The authors suggested a hole transport mechanism through the bulk and a surface barrier of a "leaky" TiO_2 due to defects in the bulk of the amorphous TiO_2 and Ni intermixing at the surface.[8,21] Thermal annealing of the amorphous TiO_2 drastically reduced its performance, indicating that crystallization is detrimental, and Hu et al.[8] suggested that upon annealing charge transport of holes relies on tunneling in insulating, crystalline, and undoped TiO_2, which is feasible only for TiO_2 films with thickness <2 nm.[10,15,22] These results, however, are rather encouraging, and correct understanding of the charge carrier transport in anodic TiO_2 protection layers can lead to

Received: May 7, 2015
Revised: June 5, 2015

DOI: 10.1021/acs.jpcc.5b04407
J. Phys. Chem. C XXXX, XXX, XXX−XXX

substantial progress in the development of efficient photoelectrochemical tandem cells.

Here, we describe the charge carrier transport properties of thick, crystalline, transparent, and intrinsically doped n-type TiO_2 films in an photoanode assembly based on the current knowledge available for cathodic n-type TiO_2 protection layers.[16] The experimental results and theoretical band diagram calculations provided here for TiO_2-protected Si photoanodes show that charge carrier transport relies solely on an electron transport mechanism through the states near the conduction band of the crystalline TiO_2. This description relies on basic solid state physics principles and simplifies the understanding of TiO_2 protection layers by providing evidence that a suitable band alignment in TiO_2-protected photoanode assemblies can be easily achieved, allowing TiO_2 to act like a simple ohmic contact or transparent conductive oxide (TCO). Although Si as photon absorber and Pt as OER catalyst are used in this study due to their known properties, these requirements are generic and can be transferred to other large and small band gap photon absorbers and oxygen evolution reaction (OER) catalysts.

■ EXPERIMENTAL SECTION

Preparation of Electrodes. The np$^+$-silicon wafers used in this study were prepared in a similar manner as previously used np$^+$-silicon substrates.[19,20] Standard single-side polished n-type silicon wafers (phosphorus doped to a specified resistivity of 1−20 ohm-cm) with a thickness of 500 μm ± 25 μm grown in a Czochralski process (Topsil A/S) were used, and highly doped p-type regions were created in a predeposition process in an atmospheric pressure tube furnace in close proximity with BoronPlus planar diffusion sources (Techneglas, Perrysburg, OH, USA). The wafers were inserted into (and later extracted from) the furnace at 700 °C. The temperature was ramped up to 1025 °C at a rate of 10 °C/min in 0.1 SLM oxygen and 8 SLM nitrogen. Three micrometer tall mesas on the front of the wafer were defined by UV lithography followed by a 3 μm deep RIE etch after removal of the boron phase layer in buffered hydrofluoric acid (bHF) for 5 min and removal of the dopant on the backside (unpolished) of the wafer in a reactive ion etching (RIE) process (Pegasus, SPTS Technologies). Another batch of np$^+$-Si substrates was prepared at 975 °C (denoted np$^+_{(\text{low doping density})}$-Si) instead of 1025 °C boron predeposition temperature.

TiO_2, Pt, and Ir/IrO_x thin films were sputter deposited as described previously.[16,18−20] The crystalline 100 nm thick TiO_2 films were prepared after the Si substrate had been sputter-cleaned in an Ar atmosphere at 35 W for 120 s to remove any adventitious carbon and surface oxides. The in situ 100 nm TiO_2/5 nm Ti/p$^+$n Si electrodes were made by taking a p$^+$n Si wafer and heating it to 400 °C. Then 5 nm of Ti was deposited followed by 100 nm of TiO_2 at 3 mTorr (50 sccm of Ar and 3 sccm of O_2). We, however, note that the exact conditions to prepare transparent, crystalline TiO_2 films with high intrinsic doping densities might vary depending on the equipment used. After the samples had cooled to room temperature, either Pt thin films, Pt islands, or 7 nm Pt films were sputter-deposited at room temperature. Pt islands were prepared on a masked TiO_2-modified np$^+$-Si substrate by sputter-depositing 20 nm of Pt. The deposition is done through a shadow-mask created by a 350 μm thick Si wafer with a 200 nm silicon nitride layer. The pattern, through which the metal is deposited, is created in this nitride layer using a combination of standard UV lithography and reactive ion etching. Subsequently, holes were etched all the way through the wafer with KOH etching to reveal the patterned nitride areas. For the deposition of Ir/IrO_x, first a 4 or 8 nm thick Ir metal film was deposited in Ar plasma (5 mTorr, 30 sccm Ar) at 300 °C.[20] Subsequently, IrO_x was deposited by reactive sputtering of Ir in Ar/O_2 plasma (5 mTorr, 20 sccm Ar, 5 sccm O_2) at 300 °C.[20] Pt nanoparticles (~5 nm in diameter) were deposited by means of a simple drop-casting procedure described previously.[16] Pt thin films deposited immediately onto the p$^+$n Si substrates were prepared after the samples had been cleaned as described above.

All Si substrates were contacted at the backside by scratching Ga−In eutectic (Aldrich) and inserting a copper wire into the eutectic; the process is described in detail elsewhere.[13,16] Afterward, the back contact was sealed using hot glue (Bosch). The illuminated area at the front side (0.196 cm^2) was defined with Teflon tape. All electrodes were cleaned immediately before electrochemical measurements by Piranha solution (3:1 H_2SO_4/H_2O_2 mixture) and thoroughly rinsed with ultra-pure water (18.2 MΩ cm) afterward.

Characterization. X-ray photoelectron spectroscopy (XPS) and ultraviolet photoelectron spectroscopy (UPS) were performed with a Thermo Scientific Theta Probe instrument equipped with a monochromatized Al Kα (1486.7 eV) source and a He discharge lamp (HeI was used). The analysis of the surface morphology of the Pt island samples was performed by scanning electron microscopy in a FEI Quanta 200 FEG. Scanning of the sample surface was performed at an acceleration voltage of 5 kV. Glancing incident angle X-ray diffraction data were taken using Cu Kα radiation λ = 1.5418 Å (PANalytical X'Pert Pro), and a Varian Cary 1E UV−vis spectrophotometer was used to record optical transmission spectra of the TiO_2 thin films.

Band Diagram and Tunneling Calculations. The band diagrams are calculated at open circuit conditions in the dark and under illumination. Parts of this band diagram have already been calculated in our previous works,[17] but for completeness the entire band diagram is shown in the Supporting Information.

Tunneling currents J_t at the p$^+$Si−Ti interface and the TiO_2−Pt interface were calculated using the Wentzel−Kramers−Brillouin (WKB) approximation on a triangular tunnel barrier given by

$$J_t = eN_A \nu_{th} \exp\left(-\frac{4}{3} W_t \sqrt{\frac{2m_{eff}\Phi_B e}{\hbar^2}}\right) \tag{1}$$

where ν_{th} is the thermal velocity (10^7 cm/s at room temperature), $\hbar$ is the Planck constant divided by 2π, and m_{eff} is the effective mass of holes in Si ($0.16m_0$, where m_0 is the mass of the electron in vacuum, 9.11×10^{-31} kg[23]) and the effective mass is 7.3×10^{-31} kg[24] in TiO_2. Here W_t is the width of the triangular tunnel barrier; because the barrier is not exactly triangular, the width can only be estimated, and to a first approximation we take $W_t = W_{SB}$, which is reasonable for lower kinetic energy carriers, whereas for carriers with a higher kinetic energy a thinner barrier $W_t = W_{SB}\Phi_B/(2V_{Bi,SB})$ may be more accurate. The depletion width W_{SB} is given by

$$W_{SB} = \left(\frac{2\varepsilon_s\varepsilon_0}{eN_A} V_{Bi,SB}\right)^{1/2} \tag{2}$$

DOI: 10.1021/acs.jpcc.5b04407
J. Phys. Chem. C XXXX, XXX, XXX−XXX

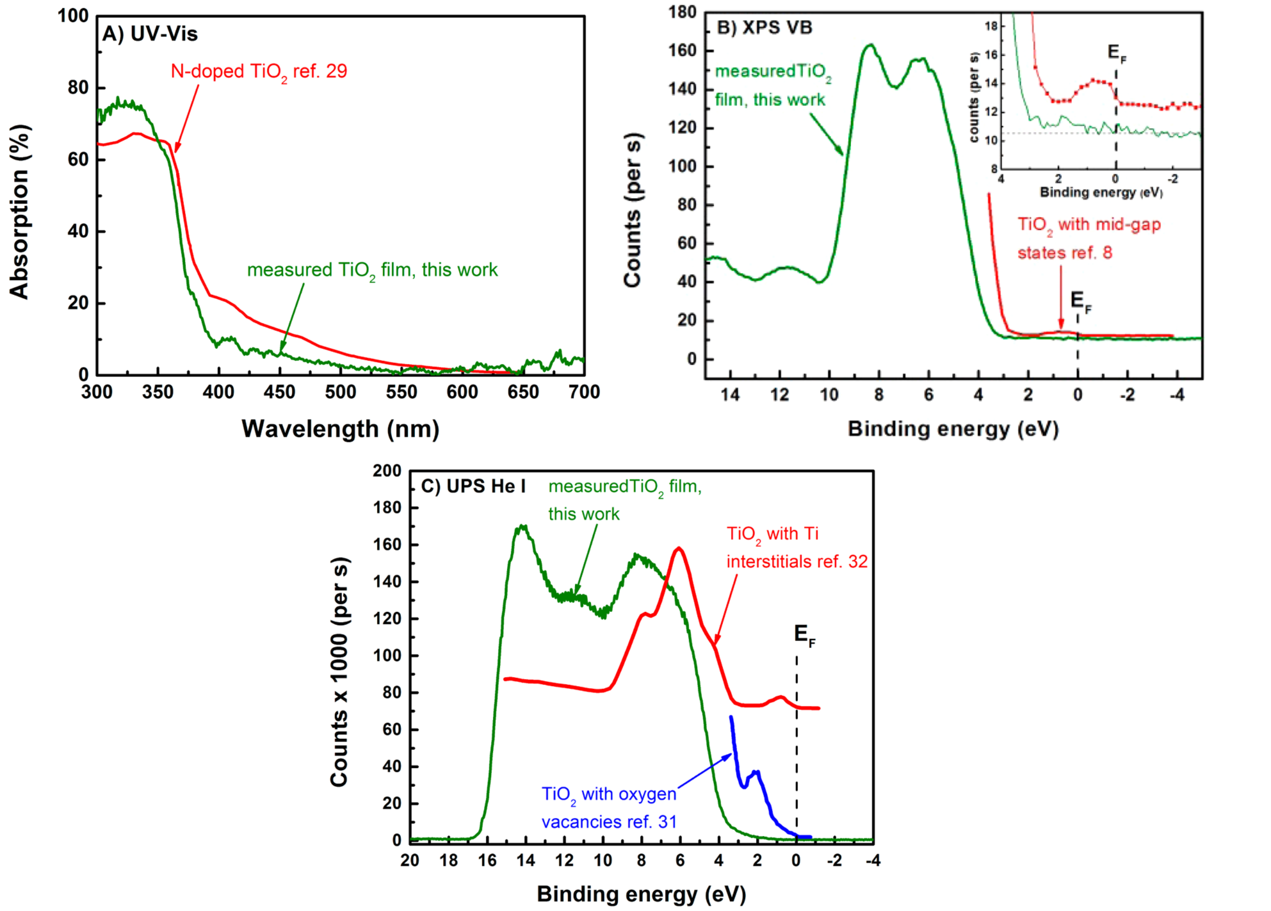

Figure 1. Characterization of sputter-deposited TiO_2 films: (A) UV−vis measurement of the sputter-deposited TiO_2 film (to exclude nitrogen doping); (B, C) valence band spectra of sputter-deposited TiO_2 films [(B) X-ray photoelectron valence band spectra of the crystalline TiO_2 film prepared by in situ sputter deposition to exclude the presence of mid-gap states in the VB (inset, zoom in of the relevant region between −3 and 4 eV); (C) UPS (HeI) valence band spectra of the crystalline TiO_2 film prepared by in situ sputter deposition (to exclude the existence of Ti interstitials or oxygen vacancies)].

where ε_s is the relative permittivity ($\varepsilon_s = 11.8$ for Si or $\varepsilon_s = 75$ for TiO_2), $\varepsilon_0 = 8.85 \times 10^{-12}$ Fm^{-1} is the vacuum permittivity, and $V_{Bi,SB}$ is the built-in voltage of the Schottky barrier junction.

RESULTS AND DISCUSSION

To investigate the charge carrier transport mechanism in TiO_2-modified photoanodes, degenerately doped Si and homojunction np^+-Si substrates were coated with TiO_2 films by sputter deposition.[16] The sputter-deposited TiO_2 was shown to produce crystalline anatase phase TiO_2 films, confirmed by X-ray diffraction (XRD) (Figure S1), while completely covering the surface with the Si (as confirmed by XPS (Figure S2) with a high intrinsic doping density, allowing electronic conduction throughout the TiO_2.[16,17,25,26] It should be noted that although it is typically described that TiO_2 transports electrons through the conduction band, it is highly likely that electrons are actually transported by polaron hopping between Ti^{3+} trap states and Ti^{4+} states.[27] Given that the trap states are very near (~0.3 eV)[27] in energy to the conduction band states, modeling the electronic transport with regard to energy levels via conduction band should thus be a reasonable approximation. (Modeling quantitative ohmic resistance through the TiO_2 would be a much more complicated issue.) To ensure that any trap states are located only near the conduction band and are not deep midgap states contributing to the charge transport properties of the crystalline TiO_2 films,[8] the electronic structure of the sputtered TiO_2 films was thoroughly characterized. The optical band gap of the 100 nm thick TiO_2 film was confirmed to be 3.2 eV, and no pre-edge absorption features were observed, indicating the absence of optically active midgap states (Figure 1A). The band gap of the TiO_2 film was additionally confirmed by XPS and UPS measurements of the TiO_2 valence band region (Figure 1B,C). Consistently, the good agreement between the optical band gap and the band gap from valence band region UPS measurements confirm a Fermi level, which is close to the conduction band edge of the TiO_2 thin film. The presence of partially filled defect states in the TiO_2 band gap can be excluded as no additional features were observed in the XPS or UPS valence band region spectra (Figure 1B,C). As shown in Figure 1, partially filled defect or optically active states due to, for example, nitrogen[28,29] doping close to the TiO_2 valence band (red trace Figure 1A, adapted from ref 29), oxygen vacancies[30,31] (blue trace Figure 1C, adapted from ref 31), or Ti interstitials between 0 and 1.5 eV below the conduction band edge (red trace Figure 1C, adapted from ref 32) are not present in the TiO_2 band gap. Instead, the doping of the prepared TiO_2 films is solely due to an intrinsic doping of active ionized donor states close to the conduction band[33,34] with a bulk doping density of $N_{D,TiO2} = 5 \times 10^{19}$ cm^{-3} and a flat band potential of $E_{FB} = -0.02$ V versus RHE measured by Mott−Schottky analysis, which was previously

DOI: 10.1021/acs.jpcc.5b04407
J. Phys. Chem. C XXXX, XXX, XXX−XXX

Scheme 1. Band Diagrams of an np$^+$Si/5 nm Ti/100 nm TiO_2/Pt Film Photoelectrode:[a] (A) Overall Band Diagram at an Applied Bias of 1.4 V versus RHE under Illumination Highlighting, in Red, the Interfaces That Are Considered To Be Important in a TiO_2-Protected Photoanode; (B) Zoom in of the p$^+$-Si−Ti Interface;[b] (C) Zoom in of the TiO_2−Pt−Electrolyte Interface from the Overall Band Diagram Shown in (A)[c]

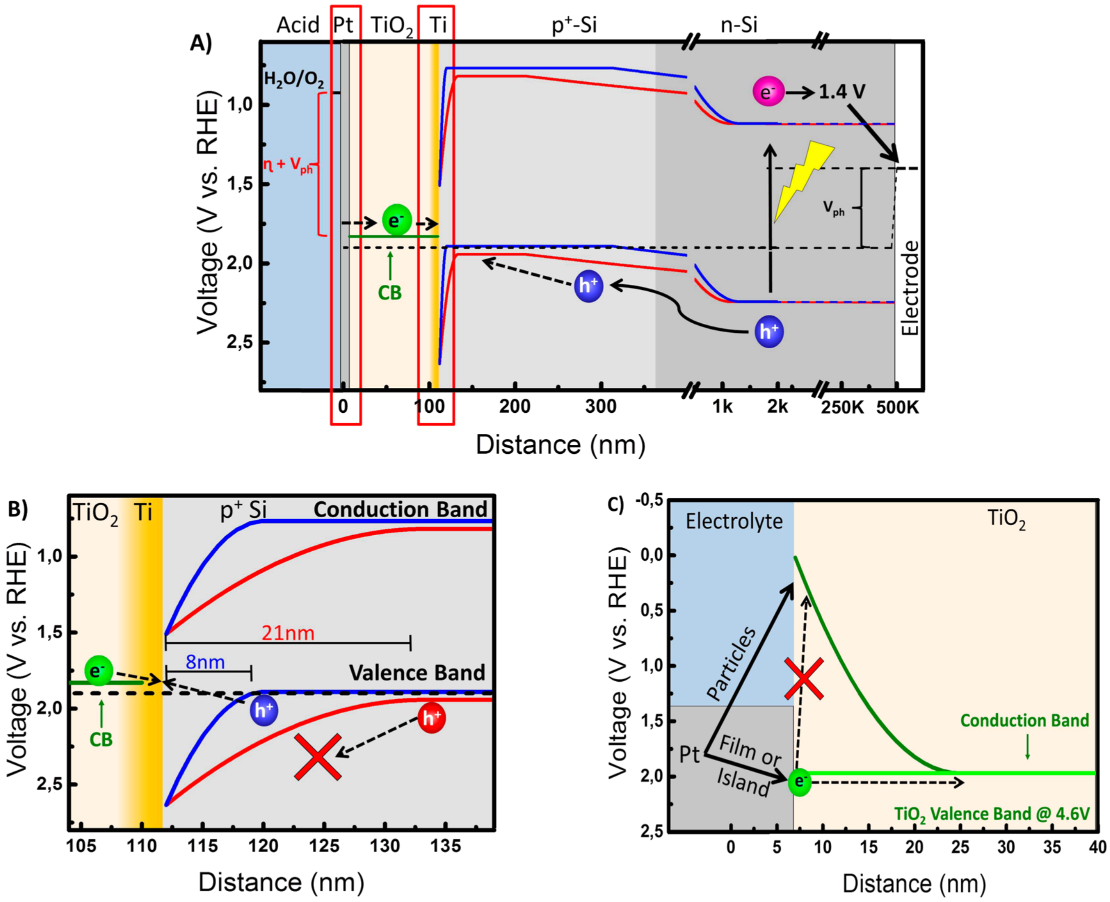

[a]A similar band diagram for a TiO_2-protected photocathode was previously reported.[16] [b]The blue and red lines represent np$^+$-Si substrates with p$^+$-layer doping densities of $N_A = 1.5 \times 10^{19}$ cm^{-3} (blue line) or $N_A = 2 \times 10^{18}$ cm^{-3} (red line), respectively. The conduction band of TiO_2 is denoted CB. [c]This scheme shows how the TiO_2 band diagram varies whether the Pt is a film, an 8 μm island, or ∼5 nm nanoparticles. The band diagrams are drawn to scale.

reported for similarly deposited 100 nm TiO_2 films.[35] Thus, the characterization shows that the TiO_2 used in this study is an n-type semiconductor and charge transport will be realized through the conduction band of TiO_2. Conversely, defect states between 0 and 2 eV below the conduction band edge (Figure 1B, red trace), as observed by Hu et al.,[8] enabling a hole transport mechanism are not observed in this work.

In Scheme 1 the complete band diagram of the TiO_2-protected photoanode assembly under irradiation is schematically shown assuming a Schottky barrier at the p$^+$-Si−Ti interface, an ohmic contact at the Ti−TiO_2 interface, an ohmic or semiconductor−electrolyte interaction at the TiO_2−Pt interface, and an electron transfer throughout the conduction band of TiO_2 [see Scheme 1C; for a more detailed calculations and a band diagram without illumination see the Supporting Information (Figure S3)]. As highlighted, the interface between the Si substrate and the Ti/TiO_2 film (Scheme 1B) as well as the interface between the TiO_2 film and the electrolyte (Scheme 1C) can be considered important as charge transport barriers might exist at these interfaces. Thus, on the basis of these diagrams it will be shown experimentally that TiO_2 can behave as a simple electron conductor even when it serves as a protection layer for Si-based photoanodes, and the requirements which the two highlighted interfaces must fulfill will be pointed out. Whereas Si as photoabsorber and Pt as OER catalyst are mainly used in this study due to their known properties and preparation procedures, these requirements are generic and can be transferred to other large and small band gap photon absorbers and OER catalysts. Thus, even though the design presented here is not an energy-saving system, it can be understood as a model system for a variety of TiO_2-protected photoanodes.

The applicability of TiO_2 films was first tested for dark electrochemical OER (Figure 2A) activity using Si/Ti/TiO_2/Pt electrode assemblies with compact Pt films. Degenerately doped p$^+$-Si, imitating the interface in a homojunction np$^+$-Si photoanode was used as substrate to avoid energy barriers at the Si/Ti/TiO_2 interface (OER activities of Si/Ti/TiO_2/Pt electrode assemblies prepared on degenerately doped n$^+$-Si are shown in Figure S4). Additionally, the compact, sputter-deposited Pt metal film ensures an ohmic-like contact with the TiO_2 surface,[36−40] whereas band bending at the TiO_2/electrolyte interface in the TiO_2 is avoided by electrostatic screening (not "pinched-off").[16,24] Thus, charge transport

DOI: 10.1021/acs.jpcc.5b04407
J. Phys. Chem. C XXXX, XXX, XXX−XXX

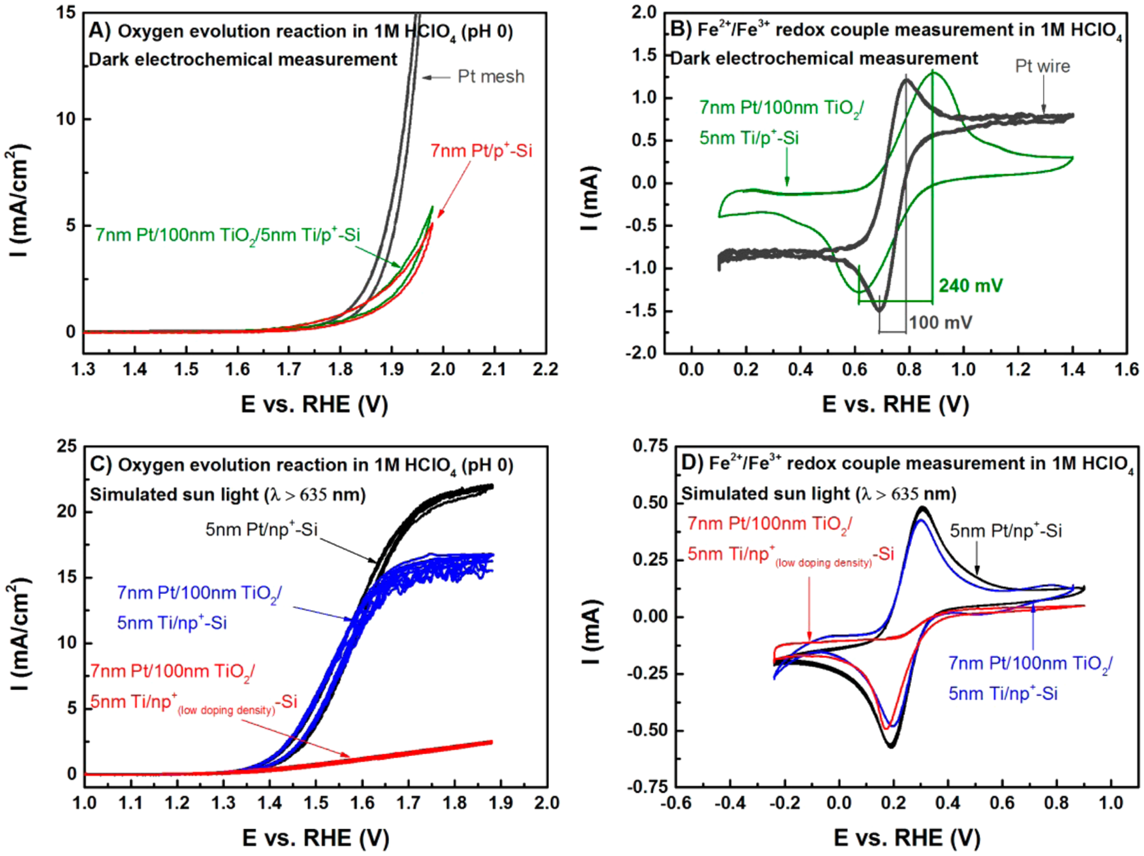

Figure 2. (A) Current−voltage behavior of degenerately doped p^+-Si substrates modified by either 7 nm Pt films or a stack of 5 nm Ti/100 nm TiO_2/7 nm Pt films measured in the dark in 1 M $HClO_4$. For comparison, the current−voltage behavior of a Pt mesh is added. The data are normalized to geometric surface area. (B) Behavior of a similar p^+-Si/Ti/TiO_2/Pt electrode in contact with a 10 mM Fe(II)/Fe(III) redox couple in 1 M $HClO_4$. (C) Photoelectrochemical behavior of differently modified np^+-Si photoanodes in 1 M $HClO_4$ under illumination with simulated sunlight (λ > 635 nm, AM 1.5G) showing the importance of the p^+-layer doping density. (D) Behavior of similar Si-photoanodes in contact with a 10 mM Fe(II)/Fe(III) perchlorate redox couple in 1 M $HClO_4$ under illumination with a Hg lamp using a cutoff filter (λ > 635 nm). The $np^+_{(\text{low doping density})}$-Si substrate was prepared at 975 °C (instead of 1025 °C) during the boron (i.e., p^+) predeposition step. The data were not cell resistance compensated.

within the thick crystalline TiO_2 interlayer can be addressed exclusively. For comparison, the OER activities of samples without the TiO_2 layers, such as degenerately doped p^+-Si/7 nm Pt electrodes, and a Pt mesh are also included in Figure 2A. The results indicate that both p^+-Si/Ti/TiO_2/Pt (Figure 2A, green trace) and p^+-Si/Pt (Figure 2A, red trace) electrode assemblies can drive the oxygen evolution at a threshold and with current densities close to those of the reference Pt mesh (Figure 2A, gray trace). Despite the thick, crystalline TiO_2 protection layer in the p^+-Si/Ti/TiO_2/Pt electrode, no significant losses compared to the p^+-Si/Pt were observed, and hence the TiO_2 film can be considered as a generic electron-conducting layer. Whereas the high overpotential and the low efficiency for catalyzing OER are consistent with the fact that Pt is a poor OER catalyst compared with Ir, Ru, and their oxides,[41] the results indicate that charge transport throughout the TiO_2 film is feasible without any major internal resistance losses. Thus, utilizing better OER catalysts would likely result in a lower OER overpotential without changing the working principle of the Si/Ti/TiO_2/Pt electrode assemblies.

The electronic transport across the interfaces in the p^+-Si/Ti/TiO_2/Pt electrode was further characterized using an electrolyte solution containing an Fe(II)/Fe(III) redox couple in 1 M $HClO_4$. The electrochemical characterization confirmed that both oxidation and reduction of the facile Fe(II)/Fe(III) redox reactions can be performed independently (Figure 2B). With a half peak-to-peak splitting of 120 mV for the Si/Ti/TiO_2/Pt electrode assembly, the electrode performance is similar to a Pt wire reference showing a half peak-to-peak splitting of ∼50 mV. This clearly indicates that only a small resistance was introduced by TiO_2 even though the electrode assemblies have a 100 nm thick crystalline TiO_2 interlayer between the Si substrate and the compact Pt film. Thus, the electrode is able to mediate the bidirectional charge transport to and from the silicon substrate through the TiO_2 to the Pt film with only minor losses, and the TiO_2 film can be considered as a simple ohmic contact in this electrode assembly. Finally, the ohmic conduction behavior of the TiO_2 films was confirmed for Si/Ti/TiO_2/Pt assemblies prepared on degenerately doped n^+-Si instead of a p^+-Si substrate (shown in Figure S4), evidencing the versatility of the TiO_2 protection strategy.[16,42]

For photoelectrochemical OER testing, the Ti/TiO_2/Pt stack with a compact 7 nm Pt film was deposited on a photoactive np^+-Si substrate (Figure 2C). Water oxidation was performed in 1 M $HClO_4$ acid solution under irradiation with a Xe lamp using an AM 1.5G filter and a 635 nm cutoff filter so as to use only the low photon energy light spectrum (Figure S5), because in a real device, the high-energy photons (blue part of the light spectrum) are reserved for the high band gap

DOI: 10.1021/acs.jpcc.5b04407
J. Phys. Chem. C XXXX, XXX, XXX−XXX

photoelectrode.[43] For the np^+-Si/5 nm Pt electrode without a TiO_2 layer (Figure 2C, black curve) current densities of 1 mA/cm^2 were obtained at an applied bias 1.4 V versus RHE (corresponding to a surface bias of 1.9 V versus RHE, due to the photovoltage (~500 mV) of the np^+-Si) with a Tafel slope of ~145 mV/dec, which is in good agreement with previous reports of Pt OER catalysts.[15,41] The photoelectrochemical performance for a Si-based np^+-homojunction photoanode modified with the $Ti/TiO_2/Pt$ film stack (Figure 2C, blue curve) is observed to closely resemble the performance of the simple np^+-Si/5 nm Pt reference electrode (Figure 2C, black curve), similar to the dark electrochemical measurements (Figure 2A) except naturally for the 500 mV shift due to the photovoltage. Likewise, the electrochemical measurements in an aqueous electrolyte of 10 mM Fe(II)/Fe(III) perchlorate redox couple (Figure 2D) evidenced that oxidation and reduction of Fe(II)/Fe(III) can be performed at both the np^+-Si/Ti/TiO_2/Pt and the np^+-Si/5 nm Pt electrodes.

Additionally, by using compact IrO_2 thin films instead of compact Pt films, the versatility of the electron-conducting TiO_2 layer to other OER catalysts was shown (Figure 3). The

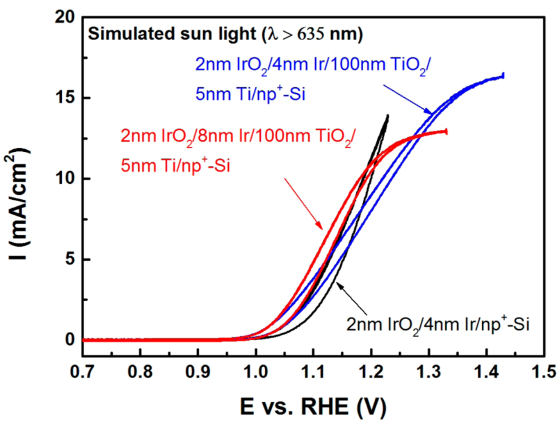

Figure 3. Behavior of Ir/IrO_2-modified photoanodes. The photoelectrochemical measurements were performed in 1 M H_2SO_4 under illumination with simulated sunlight (λ > 635 nm, AM 1.5G). Data were not corrected for solution resistance.

TiO_2-modified Si-photoanodes covered with Ir/IrO_2 thin films were tested to verify that the modified Si-photoanode can also be used with better OER catalysts than Pt. IrO_2 was used due to the relatively small overpotential for the OER. Two different Ir/IrO_2-modified electrodes with varying Ir/IrO_2 thicknesses (2 nm IrO_2/4 nm Ir and 2 nm IrO_2/8 nm Ir) were used. For comparison, the results obtained for a 2 nm IrO_2/4 nm Ir/np^+-Si photoanode are also shown. As expected, a cathodic shift in OER onset potential was observed due to the lower overpotential of IrO_2 OER catalysts. Obviously, there are only small differences between the different Ir/IrO_2 thin film modified Si-photoanodes. Whereas the photocurrent onset potentials for Ir/IrO_2 modified np^+-Si/5 nm Ti/100 nm TiO_2 are similar, the Tafel slope of the 2 nm IrO_2/8 nm Ir resembles the slope of the 2 nm IrO_2/4 nm Ir/np^+-Si reference electrode, but the slope of the thinner 2 nm IrO_2/4 nm Ir is slightly worse and a higher overpotential is required to obtain current densities of 10 mA/cm^2. Interestingly, a cathodic shift in the onset potential of the oxygen evolution potential was observed for the np^+-Si photoanode modified by the TiO_2 film. This may be due to variations in surface states (i.e., less recombination) at the Ti–Si interface compared to the Ir–Si interface. However, the results show that the np^+-Si/5 nm Ti/100 nm TiO_2 electrodes can be modified by other OER catalysts. Thus, the charge transport is independent of the OER catalyst used, provided that they are sufficiently conductive, and feasible for the dark electrodes and for the np^+-Si photoanodes, even through a thick crystalline TiO_2 layer without heteroatom doping.

Interestingly, the doping density of the Si p^+ layer and thus the interface between the Si substrate and the Ti/TiO_2 films (where a hole from the silicon must annihilate an electron from the CB of the TiO_2) is critical to the capability of the photoanode assembly to perform oxygen evolution. Tunneling calculations show that a short depletion length (<10 nm) for the p^+-Si should allow for electronic tunneling (for further information see the Supporting Information). However, these calculations also show that even a small decrease in the p^+-doping density (from 2×10^{19} to 1×10^{19} cm^{-3}) can decrease the tunneling current by many orders of magnitude. Thus, it is essential that the p^+ layer is highly doped to minimize depletion width and to accommodate significant tunneling currents (Scheme 1B). Experimentally, the effects of a lower doped p^+ Si were investigated using the $Ti/TiO_2/Pt$ stack on a np^+-Si substrate by performing the boron predeposition step at a furnace temperature of 975 °C instead of the standard 1025 °C. The result is a decrease in the p^+-doping level from 1.5×10^{19} to 2.0×10^{18} cm^{-3} in the sample prepared at 975 °C (Figure S6), corresponding to an increase in depletion layer width from 8 nm (1025 °C sample) to 21 nm for the 975 °C sample. Using these depletion widths as the tunnel barrier thickness, the maximum tunneling current density for the 975 °C samples could be estimated to be 1×10^{-12} mA/cm^2, whereas the maximum current density for the 1025 °C sample is ~10^2 mA/cm^2. As expected, using the lower doped p^+ layer allowed only minimal tunneling current, which resulted in minimal O_2 evolution current (Figure 2C, red trace), and oxidation of Fe(II) to Fe(III) in the Fe(II)/Fe(III) redox couple measurements is not possible with the Si substrate with the low boron doping density (Figure 2D, red trace). Interestingly, the reduction wave of Fe(III) to Fe(II) is still observed, which is counterintuitive and has to be further explored.

Another key to enable pristine n-type oxides to work for protecting (photo)anodes is to ensure the electron transfer from the OER catalyst into the conduction band of the TiO_2 film, which is certainly fulfilled by sputter-deposited compact Pt films, which are in good electronic contact with TiO_2 (Scheme 1C).[36−40] Due to device cost and for an efficient light harvesting in a tandem device, however, it might be required that particles rather than compact light-absorbing films be used as OER catalysts. The applicability of differently sized Pt domains and their charge transport properties were investigated by geometric size of the individual TiO_2–Pt junctions on the samples ranging from Pt nanoparticles (~5 nm in diameter) to large Pt islands (8 μm in diameter; for further information see the Supporting Information). Whereas sputter deposition was employed for the preparation of Pt islands to ensure an ohmic-like contact, nanoparticular Pt (~5 nm in diameter on average) was deposited by a solution-based preparation method.

Figure 4A shows the photoelectrochemical OER performance of the np^+-Si/Ti/TiO_2/Pt (5 nm) nanoparticle and the np^+-Si/Ti/TiO_2/Pt (8 μm) island samples. The photocurrent onset for all samples is similar, and the np^+-Si/Ti/TiO_2/Pt (8 μm) islands (Figure 4A, blue trace) closely resembles the

DOI: 10.1021/acs.jpcc.5b04407
J. Phys. Chem. C XXXX, XXX, XXX−XXX

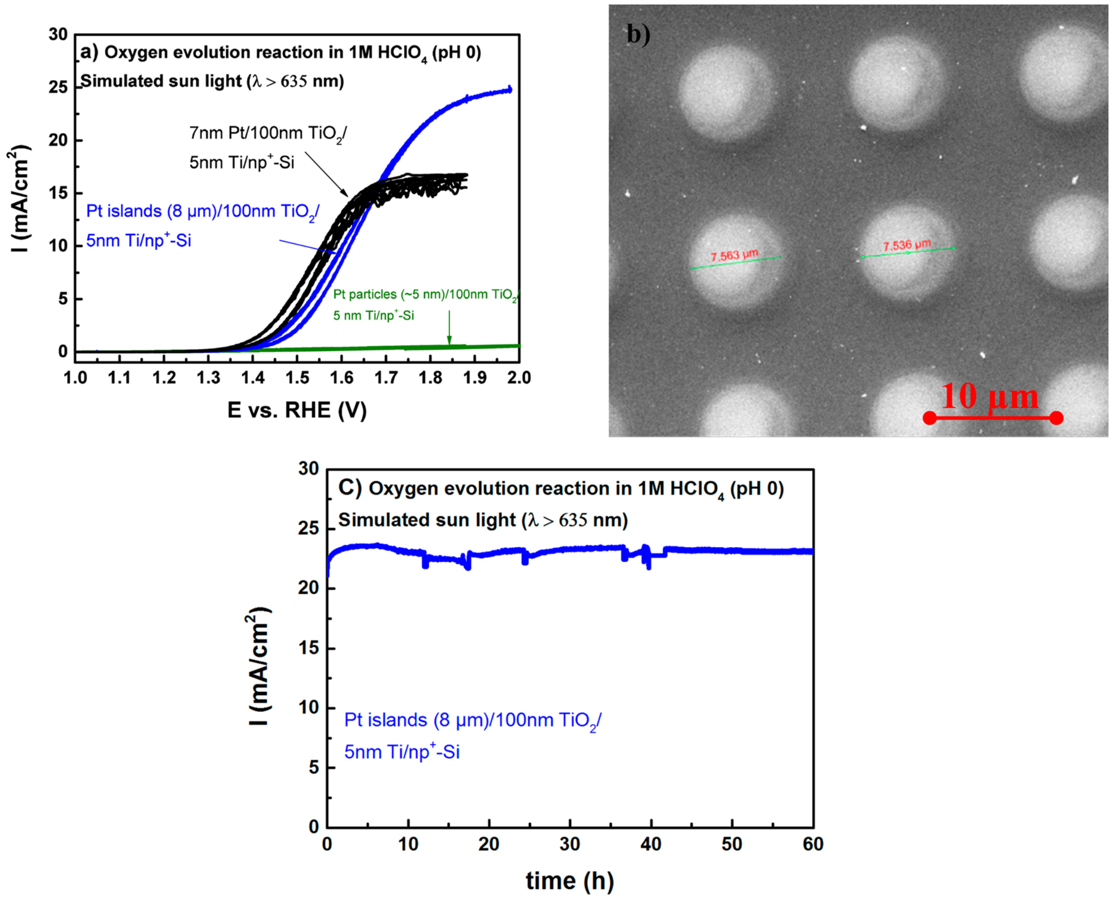

Figure 4. (a) Photoelectrochemical behavior of np$^+$-Si//TiO$_2$ photoanode modified with either Pt islands (8 μm diameter) prepared by sputter deposition or Pt particles prepared by wet-chemical impregnation. As reference, the CV curve of the np$^+$-Si/Ti/TiO$_2$/Pt 7 nm film photoanode under similar conditions is also included. (b) SEM picture of the np$^+$-Si/Ti/TiO$_2$/Pt islands photoanode. (c) Stability measurements of np$^+$-Si//TiO$_2$ photoanode modified with Pt islands (8 μm diameter). All photoelectrochemical measurements were performed in 1 M HClO$_4$ under illumination with simulated sunlight (λ > 635 nm, AM 1.5G). Data were not corrected for solution resistance.

performance of the np$^+$-Si/Ti/TiO$_2$/Pt film reference electrode (Figure 4A, black trace). Furthermore, higher saturation currents were obtained with the np$^+$-Si/Ti/TiO$_2$/Pt (8 μm) islands electrode, due to decreased reflection of incoming light as the TiO$_2$ surface is not fully covered by Pt (Figure 4B). In the case of the 5 nm Pt nanoparticle modified electrode, however, a significant resistance is observed and very high potentials are required to achieve a current density of just 1 mA/cm^2. This behavior of the Pt nanoparticular photoanode can be explained by various effects, that is, the pinch-off effect[24,44] or the formation of a Schottky barrier at the Pt−TiO$_2$ interface due to the preparation conditions. Considering an ohmic contact between the Pt OER catalysts and the TiO$_2$ film, the degree to which electrostatic screening of the TiO$_2$ surface (pinch-off effect) influences the band diagram is linearly proportional to the TiO$_2$ depletion width.[24] At an applied potential of 1.9 V versus RHE (resulting in a barrier height of 1.99 eV at the TiO$_2$−electrolyte interface and a depletion width of 18 nm, Scheme 1C), the depletion width implies that Pt nanoparticles with a diameter of only ca. 5 nm are to a large extent electronically pinched off (detailed calculations are in the Supporting Information). Therefore, in contrast to the np$^+$-Si/Ti/TiO$_2$/Pt film and np$^+$-Si/Ti/TiO$_2$/Pt island photoanodes, efficient electron transfer from the Pt nanoparticles into the TiO$_2$ might not be possible. Likewise, the photoelectrochemical behavior of the np$^+$-Si/Ti/TiO$_2$/Pt (5 nm) nanoparticle electrode in contact with the Fe(II)/Fe(III) redox couple (Figure S7) demonstrates that even the easy oxidation of Fe(II) cannot be performed on this electrode, whereas the reduction of Fe(III) to Fe(II) in the cathodic sweep is still possible. This is also in good agreement with the high resistance observed for the OER reaction. Whereas the pinch-off effect is in good agreement with the photoelectrochemical measurements for a small particle distribution, in the applied wet chemical process bigger particles might additionally be deposited on the TiO$_2$ surface. Nevertheless, similar current−voltage dependencies for the OER and Fe(II)/Fe(III) redox couple measurements can also be expected if a Schottky barrier is formed at the Pt−TiO$_2$ interface. The Schottky barrier height would be at least 0.80 eV with a depletion width of 11 nm. Although that may slightly help to mitigate the pinch-off effect, the electrons still would not be able to tunnel through the Schottky barrier as the maximum tunneling current should be 1×10^{-17} mA/cm^2 (calculated using a TiO$_2$ effective mass of 7.3×10^{-31} kg[24] in eq 1). Thus, implementation of nanoparticular OER catalysts in a photoanode device, in which thick TiO$_2$ films are working as simple electron conductors, requires detailed investigation of the relative importance of the pinch-off effect versus a Schottky barrier for the specific case. Nevertheless, the results obtained here clearly demonstrate that a good physical and electronical ("ohmic-like") contact is obtained between the oxide and the OER catalyst by sputter deposition even for Pt islands.[36−38]

DOI: 10.1021/acs.jpcc.5b04407
J. Phys. Chem. C XXXX, XXX, XXX−XXX

This specific configuration allows for efficient light harvesting while simultaneously providing robust protection of the underlying photon absorber, which is shown by extended photoelectrochemical OER measurement (Figure 2C). A constant current density of ∼22 mA/cm^2 (at 1.68 V versus RHE), with slight fluctuations due to bubble formation, is observed for an extended irradiation period of 60 h. In similar experiments on Si-based photocathodes we have already shown that severe degradation of the photoelectrode performance can be observed within a few hours (<5 h) in acidic electrolyte if insufficiently protected.[16] Therefore, it is clearly shown that the employed TiO_2 film is protecting the photon absorber, and using more efficient OER catalysts long-term stable, energy-saving photoanodes can be produced.

Although the presented electrochemical, photoelectrochemical, and characterization data, supported by band diagram calculations, confirm that in situ deposited TiO_2 protection layers are highly doped n-type semiconductors, which behave like an ohmic (electron-conducting) contact in photoanode and in photocathode assemblies,[16,42] further characterization using electrochemical impedance techniques and Hall measurements might further improve the understanding of the electron transport in TiO_2 protection layers. However, the data presented here highlight that some requirements have to be fulfilled to enable the electron transport and a hole transport through the TiO_2 film can be excluded. The requirements are a sufficiently high p$^+$ layer doping density and a well-controlled TiO_2/OER catalyst/electrolyte interface.

Therefore, rather thick (100 nm) crystalline TiO_2 films can be considered as highly transparent protection layers for the protection of photocathodes[16,42] and photoanodes, behaving like simple electron conductors in both cases. This will allow for more efficient light management in tandem devices. The good electron transport properties of TiO_2 films combined with their high transparency are rather unique for anodic protection layers (i.e., meaning protecting a photoanode from contact with the electrolyte) and can be transferred to other small or large band gap semiconductors. Because TiO_2 behaves like an ohmic contact, the conduction band (CB) will always align with the valence band (VB) of the light-harvesting semiconductor, allowing for electron and hole recombination at the interface, which is supported by basic solid state physics calculations. Nevertheless, the applicability of TiO_2 as a photoanode protection layer is only possible if the TiO_2 is sufficiently contacted to the OER catalysts as the charge carrier transport relies on the electron injection into the conduction band of the TiO_2, and unfavorable band bending in the TiO_2 film due to a Schottky barrier or the pinch-off effect should be avoided. Thus, maintaining a sufficient doping level of TiO_2 at the TiO_2/OER catalysts interface is mandatory, and complete oxidation here must be circumvented. These principles are not affected by the electrolyte used, and hence it is also applicable to alkaline conditions. The underlying principle of an electron-conducting protection layer for photoanode protection presented here is thus also applicable to other n-type metal oxides. Certainly, this work opens up a much simpler way of thinking about TiO_2 protection layers, that is, simple electron conduction, and can help guide the design of highly efficient tandem photoelectrochemical water-splitting devices.

■ CONCLUSIONS

In summary, we have investigated the charge carrier transport properties of crystalline n-type TiO_2 protection layers in Si-based photoanodes using Pt as an OER catalyst. A combined experimental and theoretical approach revealed that under certain conditions charge transport in n-type TiO_2 protection layers simply relies on an electron transfer (rather than a hole transfer) through the conduction band of TiO_2. Thus, our investigations reveal that TiO_2, even in a photoanode assembly, behaves like a simple ohmic contact. Applying basic solid state physics principles highlighted the requirements enabling this electron transfer, and it was pointed out that the OER catalysts must be in ohmic contact with the TiO_2 surface to allow the electron transfer from the OER catalyst into the TiO_2 conduction band and are easily adapted for more efficient OER catalysts, that is, IrO_2. Therefore, the TiO_2/electrolyte interface in n-type TiO_2-protected photoanodes should be well controlled, and especially contacting nanoparticular OER catalysts will be a pursued in future work. This study additionally suggests that these principles and a much simpler way of thinking about TiO_2 protection layers for stabilizing photoanodes can be used as guidelines to further develop n-type photoanode protection layers.

■ ASSOCIATED CONTENT

Supporting Information

Methods, additional discussion, and figures. The Supporting Information is available free of charge on the ACS Publications website at DOI: 10.1021/acs.jpcc.5b04407.

■ AUTHOR INFORMATION

Corresponding Author

*(I.C.) E-mail: ibchork@fysik.dtu.dk.

Author Contributions

All authors have given approval to the final version of the manuscript.

Notes

The authors declare no competing financial interest.

■ ACKNOWLEDGMENTS

B.M. acknowledges funding from the Ruhr-University Research School Plus throughout the Gateway Fellowship Initiative. K.W.J. is acknowledged for fruitful discussions and reading the manuscript. For further funding we gratefully acknowledge the Danish National Research Foundation's Center for Individual Nanoparticle Functionality (DNRF54).

■ REFERENCES

(1) Lewis, N. S.; Nocera, D. G. Powering the Planet: Chemical Challenges in Solar Energy Utilization. *Proc. Natl. Acad. Sci. U.S.A.* **2006**, *103*, 15729−15735.

(2) Gray, H. B. Powering the Planet with Solar Fuel. *Nat. Chem.* **2009**, *1*, 7.

(3) Dahl, S.; Chorkendorff, I. Solar-Fuel Generation: Towards Practical Implementation. *Nat. Mater.* **2012**, *11*, 100−101.

(4) Grätzel, M. Photoelectrochemical Cells. *Nature* **2001**, *414*, 338−344.

(5) Lewis, N. S. Toward Cost-Effective Solar Energy Use. *Science* **2007**, *315*, 798−801.

(6) Kenney, M. J.; Gong, M.; Li, Y.; Wu, J. Z.; Feng, J.; Lanza, M.; Dai, H. High-Performance Silicon Photoanodes Passivated with Ultrathin Nickel Films for Water Oxidation. *Science* **2013**, *342*, 836−840.

(7) Khaselev, O. A Monolithic Photovoltaic-Photoelectrochemical Device for Hydrogen Production via Water Splitting. *Science* **1998**, *280*, 425−427.

DOI: 10.1021/acs.jpcc.5b04407
J. Phys. Chem. C XXXX, XXX, XXX−XXX

(8) Hu, S.; Shaner, M. R.; Beardslee, J. A.; Lichterman, M.; Brunschwig, B. S.; Lewis, N. S. Amorphous TiO_{FT} Coatings Stabilize Si, GaAs, and GaP Photoanodes for Efficient Water Oxidation. *Science* **2014**, *344*, 1005−1009.
(9) Paracchino, A.; Laporte, V.; Sivula, K.; Grätzel, M.; Thimsen, E. Highly Active Oxide Photocathode for Photoelectrochemical Water Reduction. *Nat. Mater.* **2011**, *10*, 456−461.
(10) Chen, Y. W.; Prange, J. D.; Dühnen, S.; Park, Y.; Gunji, M.; Chidsey, C. E. D.; McIntyre, P. C. Atomic Layer-Deposited Tunnel Oxide Stabilizes Silicon Photoanodes for Water Oxidation. *Nat. Mater.* **2011**, *10*, 539−544.
(11) Walter, M. G.; Warren, E. L.; McKone, J. R.; Boettcher, S. W.; Mi, Q.; Santori, E. a; Lewis, N. S. Solar Water Splitting Cells. *Chem. Rev.* **2010**, *110*, 6446−6473.
(12) Sun, K.; Shen, S.; Liang, Y.; Burrows, P. E.; Mao, S. S.; Wang, D. Enabling Silicon for Solar-Fuel Production. *Chem. Rev.* **2014**, *114*, 8662−8719.
(13) Seger, B.; Laursen, A. B.; Vesborg, P. C. K.; Pedersen, T.; Hansen, O.; Dahl, S.; Chorkendorff, I. Hydrogen Production Using a Molybdenum Sulfide Catalyst on a Titanium-Protected n^+p-Silicon Photocathode. *Angew. Chem., Int. Ed. Engl.* **2012**, *51*, 9128−9131.
(14) Seger, B.; Castelli, I. E.; Vesborg, P. C. K.; Jacobsen, K. W.; Hansen, O.; Chorkendorff, I. 2-Photon Tandem Device for Water Splitting: Comparing Photocathode First versus Photoanode First Designs. *Energy Environ. Sci.* **2014**, *7*, No. 2397.
(15) Scheuermann, A. G.; Prange, J. D.; Gunji, M.; Chidsey, C. E. D.; McIntyre, P. C. Effects of Catalyst Material and Atomic Layer Deposited TiO_2 Oxide Thickness on the Water Oxidation Performance of Metal−insulator−silicon Anodes. *Energy Environ. Sci.* **2013**, *6*, 2487.
(16) Seger, B.; Pedersen, T.; Laursen, A. B.; Vesborg, P. C. K.; Hansen, O.; Chorkendorff, I. Using TiO_2 as a Conductive Protective Layer for Photocathodic H_2 Evolution. *J. Am. Chem. Soc.* **2013**, *135*, 1057−1064.
(17) Seger, B.; Tilley, S. D.; Pedersen, T.; Vesborg, P. C. K.; Hansen, O.; Grätzel, M.; Chorkendorff, I. Silicon Protected with Atomic Layer Deposited TiO_2: Conducting versus Tunnelling through TiO_2. *J. Mater. Chem. A* **2013**, *1*, No. 15089.
(18) Bae, D.; Pedersen, T.; Seger, B. J.; Malizia, M.; Kuznetsov, A.; Hansen, O.; Chorkendorff, I.; Vesborg, P. C. K. Back-Illuminated Si Photocathode: A Combined Experimental and Theoretical Study for Photocatalytic Hydrogen Evolution. *Energy Environ. Sci.* **2015**, *8*, 650−660.
(19) Mei, B.; Permyakova, A. A.; Frydendal, R.; Bae, D.; Pedersen, T.; Malacrida, P.; Hansen, O.; Stephens, I. E. L.; Vesborg, P. C. K.; Seger, B.; et al. Iron-Treated NiO as a Highly Transparent p-type Protection Layer for Efficient Si-Based Photoanodes. *J. Phys. Chem. Lett.* **2014**, *5*, 3456−3461.
(20) Mei, B.; Seger, B.; Pedersen, T.; Malizia, M.; Hansen, O.; Chorkendorff, I.; Vesborg, P. C. K. Protection of p^+n-Si Photoanodes by Sputter-Deposited Ir/IrO_x Thin Films. *J. Phys. Chem. Lett.* **2014**, *5*, 1948−1952.
(21) Sivula, K. Defects Give New Life to an Old Material: Electronically Leaky Titania as a Photoanode Protection Layer. *ChemCatChem.* **2014**, *6*, 2796−2797.
(22) Viswanathan, V.; Pickrahn, K. L.; Luntz, A. C.; Bent, S. F.; Nørskov, J. K. Nanoscale Limitations in Metal Oxide Electrocatalysts for Oxygen Evolution. *Nano Lett.* **2014**, *14*, 5853−5857.
(23) Ng, K. K. *Complete Guide to Semiconductor Devices*; McGraw-Hill: New York, 1995.
(24) Rossi, R. C.; Lewis, N. S. Investigation of the Size-Scaling Behavior of Spatially Nonuniform Barrier Height Contacts to Semiconductor Surfaces Using Ordered Nanometer-Scale Nickel Arrays on Silicon Electrodes. *J. Phys. Chem. B* **2001**, *105*, 12303−12318.
(25) Diebold, U. The Surface Science of Titanium Dioxide. *Surf. Sci. Rep.* **2003**, *48*, 53−229.
(26) Henderson, M. A. A Surface Science Perspective on TiO_2 Photocatalysis. *Surf. Sci. Rep.* **2011**, *66*, 185−297.
(27) Deskins, N. A.; Dupuis, M. Electron transport via polaron hopping in bulk TiO_2: A density functional theory characterization. *Phys. Rev. B* **2007**, *75*, No. 195212.
(28) Batzill, M.; Morales, E.; Diebold, U. Influence of Nitrogen Doping on the Defect Formation and Surface Properties of TiO_2 Rutile and Anatase. *Phys. Rev. Lett.* **2006**, *96*, No. 026103.
(29) Asahi, R.; Morikawa, T.; Ohwaki, T.; Aoki, K.; Taga, Y. Visible-Light Photocatalysis in Nitrogen-Doped Titanium Oxides. *Science* **2001**, *293*, 269−271.
(30) Chen, X.; Liu, L.; Yu, P. Y.; Mao, S. S. Increasing Solar Absorption for Photocatalysis with Black Hydrogenated Titanium Dioxide Nanocrystals. *Science* **2011**, *331*, 746−750.
(31) Tao, J.; Luttrell, T.; Batzill, M. A Two-Dimensional Phase of TiO_2 with a Reduced Bandgap. *Nat. Chem.* **2011**, *3*, 296−300.
(32) Wendt, S.; Sprunger, P. T.; Lira, E.; Madsen, G. K. H.; Li, Z.; Hansen, J. Ø.; Matthiesen, J.; Blekinge-Rasmussen, A.; Laegsgaard, E.; Hammer, B.; et al. The Role of Interstitial Sites in the Ti3d Defect State in the Band Gap of Titania. *Science* **2008**, *320*, 1755−1759.
(33) Hu, C. C. *Modern Semiconductor Devices for Integrated Circuits*; Prentice Hall: Upper Saddle River, NJ, USA, 2009.
(34) Sze, S. M.; Ng, K. K. *Physics of Semiconductor Devices*, 3rd ed.; Wiley: Hoboken, NJ, USA, 2006.
(35) Malizia, M.; Seger, B.; Chorkendorff, I.; Vesborg, P. C. K. Formation of a p−n Heterojunction on GaP Photocathodes for H_2 Production Providing an Open-Circuit Voltage of 710 mV. *J. Mater. Chem. A* **2014**, *2*, 6847.
(36) Musa, M. Z.; Sarah, M. S. P.; Shariffudin, S. S.; Mamat, M. H.; Rusop, M. A Study on Ohmic Contact of Different Metal Contact Materials on Nanostructured Titanium Dioxide (TiO_2) Thin Film. In *2010 International Conference on Electronic Devices, Systems and Applications*; IEEE: New York, 2010; pp 412−414.
(37) Yang, J. J.; Strachan, J. P.; Miao, F.; Zhang, M.-X.; Pickett, M. D.; Yi, W.; Ohlberg, D.; Medeiros-Ribeiro, G.; Williams, R. S. Metal/TiO_2 Interfaces for Memristive Switches. *Appl. Phys. A: Mater. Sci. Process.* **2011**, *102*, 785−789.
(38) Yang, J. J.; Pickett, M. D.; Li, X.; Ohlberg, D.; Stewart, D. R.; Williams, R. S. Memristive Switching Mechanism for Metal/oxide/metal Nanodevices. *Nat. Nanotechnol.* **2008**, *3*, 429−433.
(39) Schierbaum, K. D.; Wei-Xing, X.; Fischer, S.; Göpel, W. *Adsorption on Ordered Surfaces of Ionic Solids and Thin Films*; Freund, H.-J., Umbach, E., Eds.; Springer Series in Surface Sciences; Springer: Berlin, Germany, 1993; Vol. 33.
(40) Schierbaum, K.; Fischer, S.; Torquemada, M. C.; de Segovia, J. L.; Román, E.; Martín-Gago, J. A. The Interaction of Pt with $TiO_2(110)$ Surfaces: A Comparative XPS, UPS, ISS, and ESD Study. *Surf. Sci.* **1996**, *345*, 261−273.
(41) Reier, T.; Oezaslan, M.; Strasser, P. Electrocatalytic Oxygen Evolution Reaction (OER) on Ru, Ir, and Pt Catalysts: A Comparative Study of Nanoparticles and Bulk Materials. *ACS Catal.* **2012**, *2*, 1765−1772.
(42) Seger, B.; Tilley, D. S.; Pedersen, T.; Vesborg, P. C. K.; Hansen, O.; Grätzel, M.; Chorkendorff, I. Silicon Protected with Atomic Layer Deposited TiO_2: Durability Studies of Photocathodic H_2 Evolution. *RSC Adv.* **2013**, *3*, No. 25902.
(43) Hou, Y.; Abrams, B. L.; Vesborg, P. C. K.; Björketun, M. E.; Herbst, K.; Bech, L.; Setti, A. M.; Damsgaard, C. D.; Pedersen, T.; Hansen, O.; et al. Bioinspired Molecular Co-Catalysts Bonded to a Silicon Photocathode for Solar Hydrogen Evolution. *Nat. Mater.* **2011**, *10*, 434−438.
(44) Nakato, Y.; Tsubomura, H. Silicon Photoelectrodes Modified with Ultrafine Metal Islands. *Electrochim. Acta* **1992**, *37*, 897−907.

DOI: 10.1021/acs.jpcc.5b04407
J. Phys. Chem. C XXXX, XXX, XXX−XXX